Abdominal wall extraction using constrained deformable model and abdominal context

Weimin Huang, Lijie Quan, Zhiping Lin, Yuping Duan, Jiayin Zhou, Yongzhong Yang, Wei Xiong

Abstract— **Information about abdominal wall can be used for many applications from organ segmentation, registration, and surgical simulation. The challenges exist in abdominal wall extraction due to its varieties in shapes, connection to the internal organs and anterior layer edge formed between the muscle and fascia/fatty layer, which may distract the shape model. In this paper we present an approach to the posterior abdominal wall extraction using the shape model and other abdominal context, particularly with the rib-spine bone information and the wall image features. The shape model is constructed based on the training abdominal walls that are delineated manually. After bone information being extracted, the wall shape deforms from the prior shape model using the snake, which is constrained by the bone context and guided by the processed image energy map with the aim of removing distracted image features of anterior abdominal wall and the outer region from the original map. Meanwhile, an overall convex shape is maintained by limiting the angles of the contour points. The proposed approach is tested on abdominal CT data which provides encouraging results.**

I. Introduction

Extraction of abdominal wall is part of the basic steps in many medical applications such as chest examination [1], treatment and measurement [2], surgical simulation [3], organ visualization and segmentation [4-7]. It is still a tedious work for manual delineation [3,7]. Furthermore, automatic segmentation of the posterior (inside) abdominal wall is challenging because the wall tissues may connect to insider organs that have similar intensity. There may be strong edges between the muscle and fascia, and the intensity of wall tissues varies in different CT scans.

There are some works studying the automatic wall extraction from CT images. In [6], Shimizu et al used active cylinder for wall segmentation, which is further used to assist the abdominal organ segmentation. It is a simplified model of wall and there is no result reported on the wall extraction. Ding et al proposed to use Mixture of Gaussians (MoG) to model the wall voxel distribution [3], where a free form deformation was applied to extract the 3D abdominal wall. In order to build the MoG model, it used partial bone segmentation to locate wall voxel sampling. There are cases that the inner organ could be imaged with very similar intensity to the wall muscles, and bone intensity distribution can be quite different in different CT scans. In [7], an interactive wall segmentation method was presented by Wu et al to manually segment several wall slices and interpolate them to the rest slices for the whole abdominal wall segmentation. Level set with texture was used by Xu et al for anterior wall segmentation [8] with texture probability map being integrated into the model. It is difficult for posterior wall segmentation as more clutters are inside the abdominal wall. In work [9], the rib bone information was also used to partially segment the wall and organ.

In this paper, we present an approach for the automatic segmentation of posterior abdominal wall using prior shape model and context of bone localizations. The prior shape of posterior abdominal wall is learned using active shape model (ASM) and the bone including the spine and rib bone is introduced as the constraints to limit the over-deformation when the abdominal organ and wall tissue have similar CT attenuation.

II. Abdominal wall segmentation

Abdominal wall is consisted of several layers of different tissues [10]. The approach presented here includes the prior model of the abdominal wall, bone extraction and deformable model for wall extraction, where the prior shape is modeled based on ASM. The bone, especially the rib can be extracted using bone extraction. Finally, the shape deformation is conducted using the snake with the bone and shape context as constraints.

A. Pre-processing

The CT images are preprocessed through a series of techniques, including smoothing, anisotropic diffusion, contrast enhancement and down sampling to 256 x 256, which reduce the image noise while retaining the important features of the underlined structures, such as edges and lines. The pixel resolutions of the original CTs are in the range of 0.6289mm~0.7820mm.

B. Model of posterior abdominal wall

Introduced by Cootes et al [11, 12], ASM model is constructed from pre-annotated wall contours. We select N training images from the dataset (N=66 in our experiment). For a wall contour from a training image, 3 critical points with maximum curvatures are obtained and n landmark points (n=100 in our experiment) are equally spaced in between. The contour can be expressed as a $2n$ element vector, $\mathbf{x}$, where

$$\mathbf{x} = (x_1, \ldots, x_n, y_1, \ldots, y_n)^T. \quad (1)$$

All the vectors $\{\mathbf{x}_j, j = 1,\ldots,N\}$ are generated and aligned into a common coordinate system by removing the translation, rotation and scale for each shape. In order to make it easier to model the shape characteristics, Principal Component Analysis (PCA) is applied to the data. Thus, any of the training set $\mathbf{x}$ can be approximated as

*Weimin Huang, Jiayin Zhou, Yuping Duan, Wei Xiong are with the Institute for Infocomm Research, 1 Fusionopolis Way, #21-01 Connexis, Singapore 138632 (+65 6408 2516; fax: +65 64082000; email: {wmhuang, jzhou, duany, wxiong}@i2r.a-star.edu.sg).

Lijie Quan, Zhiping Lin, Yongzhong Yang are with the School of EEE, Nanyang Technological Univ, Singapore; email: ({ljquan1, ezplin, yyang8}@ ntu.edu.sg).

978-1-4244-7929-0/14/$26.00 ©2014 IEEE

$$\mathbf{x} \approx \bar{\mathbf{x}} + \mathbf{Pb}, \quad (2)$$

where $\bar{x}$ is the mean shape of the model, P contains k eigenvectors of the covariance matrix and b is a *k* dimensional vector given by

$$\mathbf{b} = \mathbf{P}^{\mathbf{T}}(\mathbf{x} - \bar{\mathbf{x}}). \quad (3)$$

The vector **b** defines a set of parameters of a deformable model controlling the modes of variation.

By using k-means method, training data$\{x_1,\ldots,x_j\}$ are partitioned into more groups, based on which, several shape models are constructed. In k-means, k=3 is used to constructed multiple models. Together with the shape model built from all data without partition, we obtain 4 shape models as the initialization of wall contour for each CT slice.

C. Bone extraction

Abdominal wall has many layers of structures and the wall anatomy is complex [10], which makes it difficult for the deformable model to optimally fit to the desired posterior wall. One of the context features that can be used to locate the posterior wall is the bone position. Direct thresholding can generate some of the bones in spine and ribs. In CT data, the rib cage bone can be captured at 175 Hounsfield unit (HU) [13]. However some organ tissues could also be segmented using the HU value. To keep the bone information only we empirically increase the threshold by 50% to 260 HU to have the dense bone segmented. It is still challenging for cartilage segmentation due to the similar CT attenuation of cartilage and muscle. In this paper we will rely on the spine and rib as context for the posterior abdominal wall shape model deformation, i.e., the bones are always located out of the posterior wall. Full bone extraction methods of the rib and spine [14, 15] can serve our purpose well.

D. Deformable model for wall fitting

The ASM model can be optimized to the wall at lung area as the chest cavity is mostly dark area. An initialization of the mean model of ASM is adjusted by fitting the shape with all bone pixels out of the shape.

Mean contour is firstly scaled down to position within the abdominal wall according to bone pixels by varying the movement and scaling iteratively and is found as the one with the maximum area. Following this, contour will move towards its normal direction until it meets a bone point. The moving depends on whether there is a bone point at the direction similar to its normal direction of the wall contour. If positive, it will move along the normal direction at a given step. Otherwise, no motion is allowed at the point. The actual movement is smoothed using Gaussian filter based on the distance that each point will be affected by its eight neighbors. For each ASM model, the process above will be applied and the resulted contour with maximum area among the 4 models will be chosen. In this way, a best fit initialization is obtained.

This process is illustrated in Figure 1. Bones and spine are shown in red while contour is shown in green. The left image shows the results of scaling down 4 different ASM shape models. The middle image shows the deformation results from position in the first one based on the bone context. In the right image, the only red contour is the one with the maximum area among the four and will be placed for later use.

Figure 1: Process of initialization using 4 ASM shape models

Before the deformation using snake, the contour is adjusted according to the bone position smoothly. As the abdominal wall may become smaller than the one in the previous slice, there may be bone points inside the contour. The contour moves those points from the bone along its normal direction. Then the snake with bone and angle constrains will be applied. Snake is a parametric contour [16, 17] that deforms based on the internal forces and image forces which also called external forces to minimize the energy function. A snake model can be written as

$$\mathrm{E}_{\mathrm{snake}} = \int_0^1 E_{intern}(x)\, ds + \int_0^1 E_{image}(x)\, ds. \quad (4)$$

Explicitly, the internal energy of snake is defined as

$$\mathrm{E}_{\mathrm{intern}}(\mathrm{x}) = \frac{1}{2}(\alpha|x'(s)|^2 + \beta|x''(s)|^2). \quad (5)$$

This term controls the tension and rigidity of the snake by varying the two weighting parameters α and β respectively. The *x′ (s)* and *x″(s)* denotes the first and second derivatives of *x(s)* with respect to the arc length *s*. The image energy is represented as a combination of energy for different image features, such as line, edge and termination, which is given as

$$\mathrm{E}_{\mathrm{image}}(\mathrm{x}) = w_{line}E_{line} + w_{edge}E_{edge} + w_{term}E_{term}, \quad (6)$$

where w_{line},w_{edge} and w_{term} denote the weights of respective energy terms. E_{line}, E_{edge} and E_{term} are expressed as follows, respectively

$$E_{line} = -\mathrm{G}_\sigma * I(x,y), \quad (7)$$

$$E_{edge} = \sqrt{I_x^2 + I_y^2}, \quad (8)$$

$$E_{term} = \frac{I_{yy}I_x^2 - 2I_{xy}I_xI_y + I_{xx}I_y^2}{(I_x^2+I_y^2)^{3/2}}, \quad (9)$$

where G_σ is a Gaussian of standard deviation σ, *I(x,y)* is the image, I_x, I_y are the first derivatives of the image with respect to x and y respectively, and I_{xx}, I_{yy} are the second derivatives of the image with respect to x and y respectively.

During each iteration, the movement of the contour is derived by calculating the first order derivatives of preprocessed image energy, which is also the image force field. In this proposed method, image energy map is preprocessed by removing the anterior abdominal wall and its outer region. The anterior abdominal wall consists of strong edges, sometimes even stronger than the posterior abdominal wall, which will attract the snake more than the posterior wall when no rib or cartilage bone is shown. Meanwhile, bone context and angle information are used to regularize the snake. If there is any bone point inside the contour, the point nearest to it on the contour will be found and its deformation step in this iteration will be set to zero. Similarly, convexity or curvature at non-spine area will be preserved as well. When

those contour points over deform, the convexity or curvature will go beyond the limit, the moving steps will be set to zero. In order to make the movement of snake smooth, the moving steps are smoothed using Gaussian filter.

When snake stops, there could be some bone points inside the contour. To make the contour deform away from bone points, contour points near those bone points move in their normal directions smoothly.

Once the first wall contour is segmented, it will be used as the initial contour for its neighboring slice.

III. Implementation Issue

A. Extract anterior abdominal wall

Strong edges, especially the anterior abdominal wall may attract snake to a local minimum. Therefore, without the bone pixel constraint, it may converge to wrong locations. Thus, it is necessary to extract the anterior abdominal wall and remove it as well as its outer region from the image energy map.

Firstly, the outermost boundary is obtained by finding points with the largest number of connected components and the rest is removed from the map. The outermost layer is the skin layer, which is the blue contour in the middle image of Figure 2. The layer has a thickness due to the smoothing operation when generating the external energy map. We used erosion morphology operation to remove the outmost skin layer. Therefore, an inner boundary can be obtained (the red contour in the middle image). In the snake energy map [16], since the coefficient used for smoothing is a constant for all CT images, the size of the erosion structuring element can be fixed at 7x7. Within the inner contour, the remaining energy map will be converted to a binary map regarding to a thresholding T=0.15. Following morphological operation to ensure the closed the boundaries in the binary map, an anterior abdominal wall can be obtained in the end.

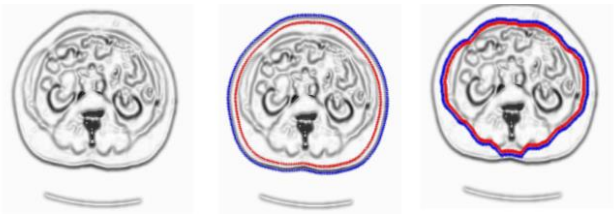

Figure 2: Anterior abdominal wall extraction process from image energy map (blue line for outer boundary and red line for inner boundary)

The whole anterior abdominal wall extraction process can be shown as Figure 2. From left to right, they are original image energy map, outmost wall extraction and anterior abdominal wall extraction. Since image energy map is generated from the smoothed edges, in the right image, the blue contour shows the outer boundary and the red contour represents the inner boundary of the anterior wall. The image energy at the anterior wall can be removed by a further morphological opening operation.

B. Maintain an overall convex shape

In order to maintain an overall convex shape, angles among points other than those being around spine are checked in each iteration. For example, for point $\boldsymbol{p_i}$, three angles are checked for robustness: angle $\boldsymbol{\theta_1}$ between point $\boldsymbol{p_{i-1}}$ and point $\boldsymbol{p_{i+1}}$, angle $\boldsymbol{\theta_2}$ between point $\boldsymbol{p_{i-2}}$ and point $\boldsymbol{p_{i+2}}$, and angle $\boldsymbol{\theta_3}$ between point $\boldsymbol{p_{i-3}}$ and point $\boldsymbol{p_{i+3}}$. These angles are obtained by

$$\theta_n = \cos^{-1}\frac{V_- \cdot V_+}{|V_-||V_+|}, \tag{10}$$

$$V_- = p_i - p_{i-n}, \tag{11}$$

$$V_+ = p_i - p_{i+n}, \tag{12}$$

where V_- and V_+ are two vectors used for angle calculation and n = 1,2,3. If θ_n is larger than 190 degree, point p_{i-n} and p_{i+n} will not move in this iteration. The angle is empirically obtained by learning from 90 slices randomly selected from different CTs. Large angle leads to too much deformation, while small angle makes snake hard to move.

IV. Experiment and Discussion

There are 6 patients' CT data (each has 64~220 images) are tested in the numerical experiments and labeled 66 wall contours are used for ASM training. Each wall contour is sampled by 100 points.

The segmentation performance is evaluated using Area Overlapped (AO), Average Distance (AD), Maximum Distance (MD) and Root Mean Square distance (RMSD) [18].

TABLE I. Segmentation Results of 6 Data Sets

Dataset	AO%	AD (mm)	MD (mm)	RMSD (mm)
1	94.99	1.1556	10.3021	1.6205
2	94.70	0.9948	6.5703	1.4026
3	93.43	1.2959	9.1213	1.9376
4	93.84	1.5020	13.5884	2.1217
5	91.48	1.3543	12.2982	1.9415
6	95.00	1.0440	7.5295	1.5412
Mean	93.91	1.2244	9.9016	1.7609

Table I summaries the results of the proposed model, which are compared with the manually labeled ground truth. The ground truth was provided by one expert. From the test, reliable posterior walls can be extracted for most of the slices despite of differences existing among datasets. In Figure 3, selected results overlapped with the ground truth from data 6 are shown. As comparison, the method in [7] achieved segmentation result with AD error from 0.71~1.27mm with STD 0.36~0.99 based on the number of selected slices labelled manually for interpolation. In our method, it is fully automatic and the mean STD is 0.67.

The small, average and minimal distances demonstrate that our method can fit to abdominal wall well, while a large maximum distance may be caused by the following three situations as shown in Figure 4. The left-most image of Figure 4 shows a common situation for segmenting CT images with no rib information. Since the edge information is quite weak, it is difficult for the snake to find the correct wall location. This may be improved using a spine model to maintain a similar shape around spine. For the middle image in Figure 4, although the edge indicated by the blue line is strong enough, snake cannot deform over due to the constraint, which try to make the shape smooth and convex on the top part of the wall.

The case shown by the right-most image sometimes happens when there is bright inner organ near the wall, such as kidney. This kind of organs has strong edges that pull snake towards them gradually and trapped onto it.

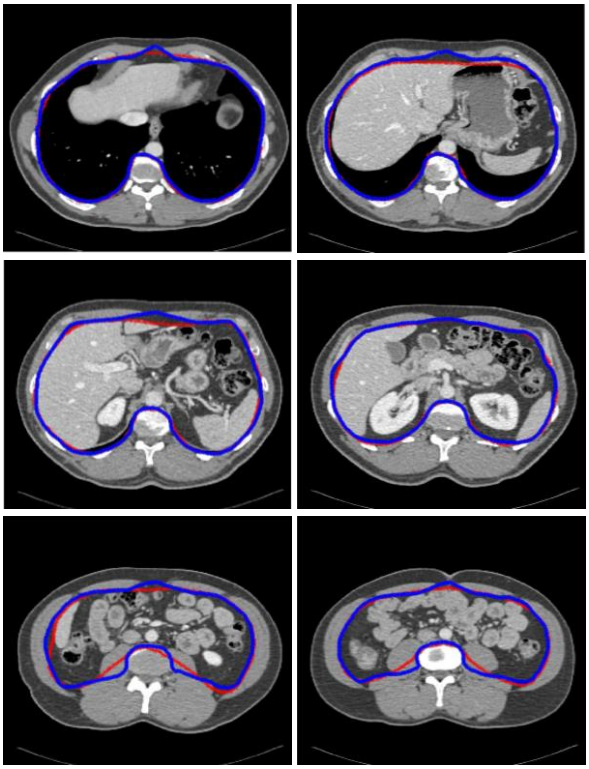

Figure 3: Comparison of our results (red line) and ground truth (blue line)

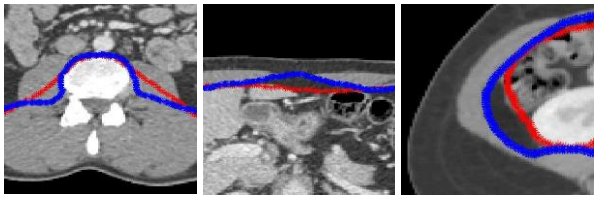

Figure 4: Detailed comparison results (red line for ours, blue line for ground truth)

The proposed method can be further improved in future works through a few approaches. Firstly, the appearance profile can be used to guide snake to a location of the real posterior wall by assigning wall edge probability, since abdominal wall has an overall dark-to-bright profile from inner to outer. In this way, snake can avoid being trapped to viscera, since its profile is generally bright-to-dark that is different from the situation of the posterior wall. Secondly, since this algorithm relies on the detection of bones including rib cage, spine, breastbone, and even costal cartilage, the efficient detection methods of these structures can improve the wall extraction. Thirdly, more accurate anterior abdominal wall extraction can be applied using the method proposed in [2].

V. Conclusion

In this paper, we proposed an intuitive approach combining snake with constraints from the bone and anterior abdominal wall contexts to segment posterior abdominal wall in CT data. The ASM prior model is used for a good initialization and snake with constraints performs for the final posterior extraction. The experimental results show that these constraints can effectively control the movement of the snake from over-deforming towards the exterior of the abdominal cavity. However, due to the nature of the snake model, being occasionally attracted to viscera is unavoidable for the proposed approach.

References

[1] N. Sverzellati, D. Colombi, G. Randi, et al, "Computed tomography measurement of rib cage morphometry in emphysems," Plos One, vol. 13, Issue 7, e68546, 2013.

[2] Z. Xu, A. Wade, B. Rebeccah, P. Benjamin and L. Bennett, "Texture analysis improves level set segmentation of the anterior abdominal wall," Medical Physics 40, 121901, 2013.

[3] J. Bano, A. Hostettler, S.A. Nicolau, S. Cotin, C. Doignon ,H.S. Wu, M.H. Huang, L. Soler, and J. Marescaux, "Simulation of Pneumoperitoneum for Laparoscopic Surgery Planning," MICCAI 2012, Part I, LNCS 7510, pp. 91–98, 2012.

[4] F. Ding, W. Leow and S. Venkatesh, "Removal of Abdominal wall for 3D visualization and segmentation of organs in CT volume," ICIP'09, pp. 3377-3380, 2009.

[5] H. Li, J. Li, S. Pan, Q. Guo, J. Liu and Y. Kang, "Automatic Rib Positioning Method in CT Images," Bioinformatics and Biomedical Engineering (iCBBE), pp.1-4, 2010.

[6] A. Shimizu, R. Ohno, T. Ikegami, H. Kobatake, S. Nawano and D. Smutek, "Segmentation of multiple organs in non-contrast 3D abdominal CT images," International Journal of Computer Assisted Radiology and Surgery, vol.2, pp.135–142. 2007.

[7] W. Zhu, S. Nicolau, L. Soler, A. Hostettler, J. Marescaux, and Y. Remond, "Fast segmentation of abdominal wall: application of sliding effect removal for non-rigid registration," Abdominal Imaging 2012, LNCS 7601, pp.198-207, 2012.

[8] Z. Xua, W. Allenb, B. Poulosec, and B. Landman, "Automatic Segmentation of Abdominal Wall in Ventral Hernia CT: A Pilot Study," SPIE-Medical Imaging, 86693T, 2013.

[9] S. Maeda, M. Komatsu, H. Kim, A. Yamamoto and K. Okuda, "Automatic Segmentation of Liver Region Employing Rib Cage and Its 3-D Displaying," SICE-ICASE International Joint Conference, pp.1465-1468, 2006.

[10] J. Skandalakis, G. Colburn, T. Weidman, R. Foster Jr, A. Kingsworth, L. Skandalakis, P. Skandalakis, P. Mirilas, "Skandalakis' Surgical Anatomy," McGraw-hill, February 1, 2004.

[11] T. Cootes, C. Taylor, D. Cooper, & J. Granham, "Active Shape Models – Their Training and Application", Computer Vision and Image Understanding, vol. 61, pp. 38-59, 1995.

[12] T. Cootes, E. Baldock and J. Graham, "An introduction to active shape models." Image Processing and Analysis, pp. 223-248, 2000.

[13] J. Lee and A. P. Reeves, "Segmentation of invidual ribs from low_dose chest CT," SPIE Medical Imaging 2010: Computer aided Diagnosis, Vol 7624, pp.76243J, 2010.

[14] J. Lee and A. P. Reeves, "Segmentation of individual ribs from low dose chest CT," SPIE Medical Imaging 2010: Computer aided Diagnosis, vol. 7624, 76243J, 2010.

[15] T. Klinder, C. Lorenz, J. Berg, S. Dries, T. Bülow, and J. Ostermann, "Automated Model-Based Rib Cage Segmentation and Labeling in CT Images," MICCAI'07, vol.2, LNCS 4792, pp. 195-202, 2007.

[16] M. Kass, A. Witkin, and D. Terzopoulos, "Snakes: Active contour models," International Journal of Computer Vision, vol. 1, no. 4, pp.321-331, 1998.

[17] C. Xu, and J. Prince, "Gradient vector flow: A new external force for snakes," IEEE Conference on Computer Vision and Pattern Recognition, pp. 66-71, 1997.

[18] Heimann et al., "Comparison and evaluation of methods for liver segmentation from CT datasets," IEEE Transaction on Medical Imaging, vol. 28, pp. 1251-1265, 2009.